# Lattice stabilities, mechanical and thermodynamic properties of $Al_3Tm$ and $Al_3Lu$ intermetallics under high pressure from first-principles calculations*

Xu-Dong Zhang(张旭东)[1,†] and Wei Jiang(姜伟)[1,2]

[1] School of Science, Shenyang University of Technology, Shenyang 110870, China
[2] School of Materials Science and Engineering, Shenyang University of Technology, Shenyang 110870, China

(Received 8 June 2015; revised manuscript received 22 September 2015; published online 20 December 2015)

The effects of high pressure on lattice stability, mechanical and thermodynamic properties of $L1_2$ structure $Al_3Tm$ and $Al_3Lu$ are studied by first-principles calculations within the VASP code. The phonon dispersion curves and density of phonon states are calculated by using the PHONONPY code. Our results agree well with the available experimental and theoretical values. The vibrational properties indicate that $Al_3Tm$ and $Al_3Lu$ keep their dynamical stabilities in $L1_2$ structure up to 100 GPa. The elastic properties and Debye temperatures for $Al_3Tm$ and $Al_3Lu$ increase with the increase of pressure. The mechanical anisotropic properties are discussed by using anisotropic indices $A^G$, $A^U$, $A^Z$, and the three-dimensional (3D) curved surface of Young's modulus. The calculated results show that $Al_3Tm$ and $Al_3Lu$ are both isotropic at 0 GPa and anisotropic under high pressure. In the present work, the sound velocities in different directions for $Al_3Tm$ and $Al_3Lu$ are also predicted under high pressure. We also calculate the thermodynamic properties and provide the relationships between thermal parameters and temperature/pressure. These results can provide theoretical support for further experimental work and industrial applications.

**Keywords:** lattice stability, mechanical properties, thermodynamic properties

**PACS:** 63.20.D–, 62.20.–x, 65.40.–b **DOI:** 10.1088/1674-1056/25/2/026301

## 1. Introduction

The $Al_3M$ trialuminide compounds with $L1_2$ structure in aluminum alloys have attracted a great deal of attention recently due to their particularly attractive characteristics including low densities, high specific strengths, very high melting points and excellent oxidation resistances.[1–6] Among them, $Al_3Sc$ is the most studied intermetallics so far, since it has a thermodynamically stable $L1_2$ structure, relatively large volume fraction, and modest coarsening rate.[1,7,8] However, the high cost of Sc limits its industrial applications. Like Sc, Tm and Lu are cheaper than Sc and can also form thermodynamically stable $L1_2$-structured trialuminide compound.[9,10] The microstructure and mechanical properties of Tm and Lu containing Al alloys have been investigated, and it has been found that Tm and Lu can improve the creep-resistance properties of Al alloys by forming $L1_2$ structure $Al_3Tm$ and $Al_3Lu$ precipitates or solid solved in the matrix.[11] The recent studies of $L1_2$ structures $Al_3Tm$ and $Al_3Lu$ mainly focused on the electronic structure and elastic constant under ground states. Tao *et al.*[12] calculated the density of states and elastic modulus at the pressure of 0 GPa using first-principles calculations. Tsvyashchenko *et al.*[9] employed the time-differential perturbed angular correlations technique (TDPAC) to measure the parameters of hyperfine interactions in known $Al_3RE$ compounds. However, to the best of our knowledge, no first-principles calculations about the relationship between pressure and lattice stability, mechanical and thermodynamic properties for $L1_2$ structure $Al_3Tm$ and $Al_3Lu$ have been performed so far. So the effects of high pressure on phase stability, elastic constants and thermodynamic properties should be discussed for the further considerations. With the development of computer science and technology, first-principles calculations have successfully predicted the physical and chemical properties of the materials.[13–21] In the present work, the first-principles calculations are performed to better clarify and understand the lattice stabilities, mechanical and thermodynamic properties for $L1_2$ structures $Al_3Tm$ and $Al_3Lu$ under high pressure.

## 2. Computational methods

The first-principles calculations are based on density functional theory (DFT) and employ the plane-wave pseudopotential total energy method as implemented in the VASP code.[22] Projector augmented wave (PAW) functions were used and exchange correlation functional was treated using the generalized gradient approximations (GGA) of the Perdew–Burke–Ernzerhof (PBE). The $k$-point meshes for Brillouin

*Project supported by the Scientific Technology Plan of the Educational Department of Liaoning Province and Liaoning Innovative Research Team in University, China (Grant No. LT2014004) and the Program for the Young Teacher Cultivation Fund of Shenyang University of Technology, China (Grant No. 005612).

†Corresponding author. E-mail: zxdwfc@163.com

© 2016 Chinese Physical Society and IOP Publishing Ltd 

zone sampling were constructed using the Monkhorst–Pack scheme. The 12×12×12 $k$-point meshes were used for $Al_3Tm$ and $Al_3Lu$. Spin polarization was considered in all calculations. The kinetic cut-off energy of 500 eV has been tested to be sufficient for convergence. The convergence of the energy was less than $1.0\times10^{-5}$ eV. Force was converged to less than $1.0\times10^{-4}$ eV·Å$^{-1}$. In order to obtain the vibrational properties, we carried out the phonon calculation by using the supercells approach and used the 3×3×3 supercells for $Al_3Tm$ and $Al_3Lu$. Real-space force constants were calculated using the density functional perturbation theory (DFPT) with the VASP code. Phonon frequencies were calculated by using the PHONOPY code.[23]

## 3. Results and discussion

In the present work, $L1_2$ structure $Al_3Tm$ and $Al_3Lu$ belong to face-centered cubic crystal structures, each with space group $Pm\bar{3}m$ (No. 221). In the unit cell, the Tm/Lu and Al atoms occupy the Wyckoff site 1$a$ (0, 0, 0) and 3$c$ (0, 1/2, 1/2), respectively. The experimental lattice parameters of $Al_3Tm$ and $Al_3Lu$ are 4.2215 Å and 4.2947 Å.[24] In order to determine the thermodynamic stabilities for $Al_3Tm$ and $Al_3Lu$, we calculate the formation enthalpies for $Al_3Tm$ and $Al_3Lu$. The calculated results are −40.4 kJ/mol and −39.1 kJ/mol for $Al_3Tm$ and $Al_3Lu$, respectively. The obtained results agree well with the available experimental values.[24] We can note that $Al_3Tm$ has a stronger thermodynamic stability than $Al_3Lu$ since $Al_3Tm$ possesses the lower values of formation enthalpy.

### 3.1. Vibrational properties and dynamical stability

The vibrational properties play an important role in determining the physical properties of solids, such as dynamical stabilities, phase transitions, electron–phonon interactions and heat conductions and so on. We calculate the phonon spectra of $Al_3Tm$ and $Al_3Lu$ and examine their dynamical stabilities. The phonon spectrum curves at arbitrary values of wave vector $q$ of the Brillouin zone (BZ) for Al, $Al_3Tm$ and $Al_3Lu$ are shown in Figs. 1 and 2. In Fig. 1, we show the phonon dispersion curves of Al. The calculated values are plotted as solid lines. The experimental data from the inelastic neutron scattering measurement[25] are plotted as circles. The calculated values are in good agreement with the experimental data, indicating that our computational method is reliable. Figure 2 shows the phonon dispersion curves for $Al_3Tm$ and $Al_3Lu$ along $\Gamma$–$X$–$M$–$\Gamma$–$R$ directions in the first Brillouin zone at 0, 50, 100 GPa. The shapes of phonon spectrum curves are similar to each other. As the unit cells of $Al_3Tm$ and $Al_3Lu$ each contain 4 atoms, there are 12 phonon branches, which contain 9 optical modes and 3 acoustic modes. Phonon calculations can provide a criterion for crystal dynamical stability and indicate structural stability through the non-appearance of mode softening. As can be seen from Figs. 2(a) and 2(b), all phonon modes have positive frequencies, indicating the dynamical stabilities of these compounds in the $L1_2$ structure at 0 GPa. The total and partial

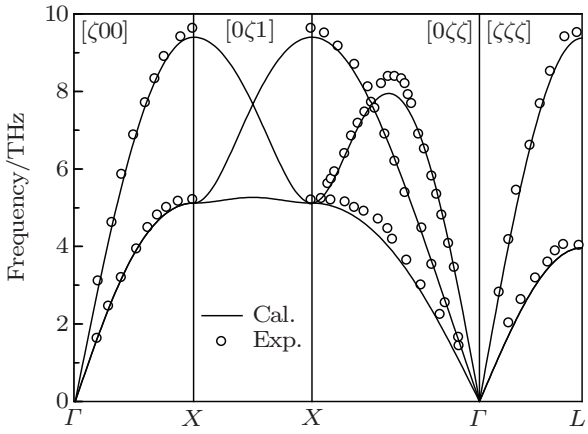



**Fig. 1.** Phonon dispersion curves of Al and the circles correspond to the experimental data.

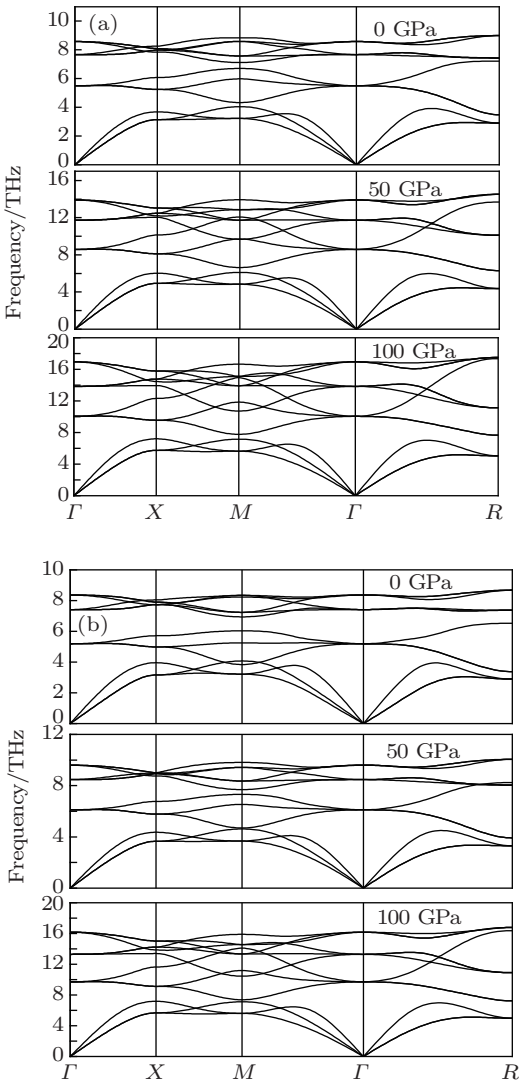



**Fig. 2.** Phonon dispersion curves for $Al_3Tm$ (a) and $Al_3Lu$ (b) under different pressures.

densities of phonon states (PHDOS) are displayed in Fig. 3. The PHDOS curves can be divided into three distinct regions. The low frequency region belongs to the acoustic modes and derives from the hybridization of the vibrational motions of Al and Tm/Lu atoms in the low frequency range of the phonon spectrum. The middle and high frequency regions result from optical modes, and are dominated by the vibration motions of Al atoms. Figure 2 also shows phonon spectra of $Al_3Tm$ and $Al_3Lu$ at 50 GPa and 100 GPa. In Fig. 2, there is neither negative frequency nor mode softening at 50 GPa and 100 GPa, indicating that $Al_3Tm$ and $Al_3Lu$ will keep $L1_2$ structure stable from 0 GPa to 100 GPa. Some numerical values at high symmetry point $\Gamma$ are listed in Table 1. When the pressure increases, we can see that most mode frequencies move up to a higher frequency and the band gap between the highest optical branches and the rest of the phonon branches has already disappeared. The phenomenon results from the shorter bond length with increasing pressure. The shorter bond can lead to the larger force constants and higher phonon frequencies.[26]

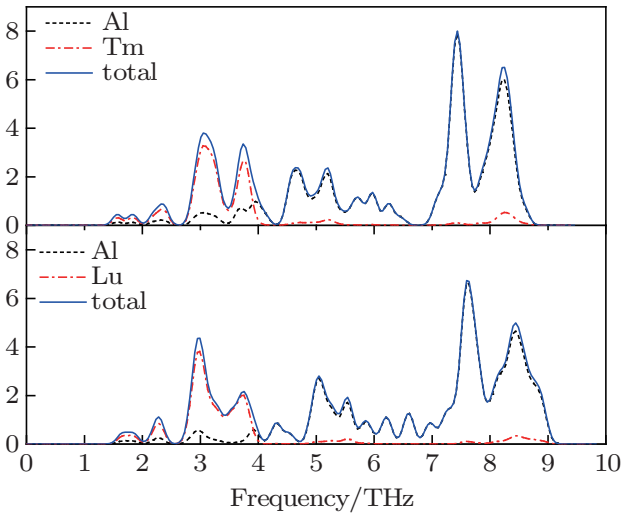



**Fig. 3.** (color online) Calculated total and partial densities of phonon states for $L1_2$ $Al_3Tm$, and $Al_3Lu$ at 0 GPa.

**Table 1.** Phonon frequencies (in THz) at the $\Gamma$ point for $L1_2$ $Al_3Tm$, and $Al_3Lu$ at different pressures (in GPa).

| Pressure | $Al_3Tm$ | | | $Al_3Lu$ | | |
|---|---|---|---|---|---|---|
| | $T_{1u}(1)$ | $T_{1u}(2)$ | $T_{2u}$ | $T_{1u}(1)$ | $T_{1u}(2)$ | $T_{2u}$ |
| 0 | 8.594 | 7.826 | 5.512 | 8.489 | 7.482 | 5.227 |
| 50 | 13.912 | 11.839 | 8.721 | 9.764 | 8.512 | 6.184 |
| 100 | 16.912 | 14.892 | 10.128 | 16.233 | 13.261 | 9.821 |

### 3.2. Elastic properties and elastic anisotropy

For elastic constants, we employ the stress-strain method proposed by Shang *et al.*[27] to calculate the elastic constants and use the Voigt–Reuss–Hill method[28] to obtain the Bulk modulus $B$, Young's modulus $E$ and shear modulus $G$. The value of bulk modulus (in GPa) $B = (B_V + B_R)/2$, where $B_V$ and $B_R$ are the Voigt's and the Reuss's bulk modulus respectively. The value of shear modulus $G = (G_V + G_R)/2$, where $G_V$ and $G_R$ are the Voigt's and the Reuss's shear modulus respectively. They are defined respectively as

$$B_V = B_R = (C_{11} + C_{12})/3, \quad (1)$$

$$G_V = (C_{11} - C_{12} + 3C_{44})/5, \quad (2)$$

$$G_R = 5(C_{11} - C_{12})C_{44})/[4C_{44} + 3(C_{11} - C_{12})]. \quad (3)$$

Using the two formulas:

$$E = 9BG/(3B + G), \quad v = (3B - E)/6B,$$

the polycrystalline Young's modulus $E$ (in GPa) and Poisson's ratio $v$ are obtained. These constants are listed in Table 2. At 0 GPa, the values of elastic properties of $Al_3Tm$ and $Al_3Lu$ are in good agreement with the previously reported results.[12] Under different pressures, the calculated elastic constants all satisfy the mechanical stability criteria, $C_{11} - C_{12} > 0$, $C_{11} > 0$, $C_{44} > 0$, $C_{11} + 2C_{12} > 0$, $C_{12} < B < C_{11}$, indicating that $L1_2Al_3Tm$ and $Al_3Lu$ will keep mechanically stable for the considered pressures ranging from 0 GPa to 100 GPa. These elastic constants and elastic moduli versus pressure are plotted in Fig. 4. The calculated values of elastic constant $(C_{ij})$ and mechanical moduli ($B$, $G$, $E$) of $Al_3Tm$ and $Al_3Lu$ exhibit similar trends and increase almost linearly with the increasing pressure. We can note that the elastic constant $C_{11}$ of $Al_3Lu$ is slightly bigger than those of $Al_3Tm$ under different pressures. Because $C_{11}$ indicates the resistance to linear compression along the $x$ direction, $Al_3Tm$ is more compressible along the $x$ axis than $Al_3Lu$. Elastic constants $C_{12}$ and $C_{44}$ are less sensitive to the increasing of pressure than $C_{11}$. Moreover, the corresponding values of elastic moduli $B$ and $G$ of $Al_3Lu$ are larger than those of $Al_3Tm$, indicating that $Al_3Lu$ is likely to be harder than $Al_3Tm$. The brittleness of the compound is related to Poisson's ratio $v$. If Poisson's ratio $v$ is less than 0.26, the compounds will be brittle materials.[29] The value of $v$ for $Al_3Tm$ increases from 0.17 to 0.214 and that for $Al_3Lu$ increases from 0.168 to 0.234 with pressure increasing from 0 GPa to 100 GPa. However, the values of $v$ of $Al_3Tm$ and $Al_3Lu$ under high pressure are still less than 0.26, indicating that $Al_3Tm$ and $Al_3Lu$ are both brittle in the whole range. The value of $B/G$ is consistent with that of $v$, which is also related to the brittleness. The critical value which classifies materials as being ductile and brittle is 1.75; i.e., if $B/G > 1.75$, the material has a ductile behavior; otherwise the material is brittle. In Table 2, these values of $B/G$ for $L1_2$ $Al_3Tm$ and $Al_3Lu$ are smaller than 1.75 with increasing pressure, suggesting that two compounds are both brittle in the considered pressure range.

**Table 2.** Elastic constants and elastic moduli (in GPa) of $L1_2$ $Al_3Tm$, and $Al_3Lu$ at different pressures (GPa).

| | $P$ | $C_{11}$ | $C_{12}$ | $C_{44}$ | $B$ | $G$ | $E$ | $v$ | $B/G$ |
|---|---|---|---|---|---|---|---|---|---|
| $Al_3Tm$ | 0[a] | 160.92 | 37.03 | 61.17 | 78.33 | 61.48 | 146.19 | 0.174 | 1.214 |
| | 0 | 161.04 | 35.39 | 64.51 | 78.27 | 65.73 | 153.89 | 0.170 | 1.192 |
| | 10 | 218.62 | 48.98 | 91.46 | 105.53 | 88.45 | 207.94 | 0.172 | 1.189 |
| | 20 | 264.13 | 64.48 | 114.10 | 131.03 | 107.49 | 254.46 | 0.176 | 1.211 |
| | 30 | 301.72 | 79.70 | 134.71 | 153.71 | 124.04 | 294.42 | 0.181 | 1.233 |
| | 40 | 338.23 | 94.80 | 153.65 | 175.94 | 139.33 | 331.89 | 0.186 | 1.257 |
| | 50 | 373.03 | 109.74 | 170.95 | 197.50 | 152.56 | 366.63 | 0.191 | 1.283 |
| | 60 | 404.65 | 124.67 | 186.84 | 218.00 | 164.43 | 398.03 | 0.196 | 1.310 |
| | 70 | 432.63 | 139.72 | 202.05 | 237.36 | 175.88 | 426.47 | 0.201 | 1.336 |
| | 80 | 459.59 | 154.91 | 216.63 | 256.47 | 186.03 | 453.5 | 0.205 | 1.363 |
| | 90 | 486.53 | 170.8 | 231.32 | 276.04 | 196.09 | 480.32 | 0.210 | 1.391 |
| | 100 | 511.11 | 185.89 | 244.91 | 294.30 | 205.16 | 504.69 | 0.214 | 1.416 |
| $Al_3Lu$ | 0[a] | 159.85 | 38.43 | 60.44 | 78.90 | 60.54 | 154.64 | 0.174 | 1.203 |
| | 0 | 162.55 | 36.18 | 65.78 | 81.97 | 69.942 | 163.36 | 0.168 | 1.172 |
| | 10 | 236.38 | 52.62 | 100.32 | 113.87 | 96.855 | 226.38 | 0.169 | 1.176 |
| | 20 | 284.23 | 70.31 | 125.01 | 141.62 | 117.448 | 276.04 | 0.175 | 1.206 |
| | 30 | 322.71 | 84.85 | 147.40 | 164.14 | 135.266 | 318.35 | 0.177 | 1.213 |
| | 40 | 362.96 | 101.70 | 167.56 | 188.79 | 151.663 | 358.89 | 0.183 | 1.245 |
| | 50 | 397.32 | 115.77 | 185.93 | 209.62 | 166.328 | 394.61 | 0.186 | 1.260 |
| | 60 | 431.00 | 133.50 | 203.50 | 232.67 | 179.492 | 428.33 | 0.193 | 1.296 |
| | 70 | 457.40 | 145.83 | 220.54 | 249.69 | 191.869 | 458.23 | 0.194 | 1.301 |
| | 80 | 489.98 | 164.50 | 237.03 | 272.99 | 203.873 | 489.71 | 0.201 | 1.339 |
| | 90 | 514.82 | 176.46 | 252.51 | 289.25 | 244.63 | 517.04 | 0.223 | 1.345 |
| | 100 | 542.50 | 192.08 | 267.83 | 308.89 | 248.91 | 544.94 | 0.236 | 1.367 |

[a]Ref. [12]

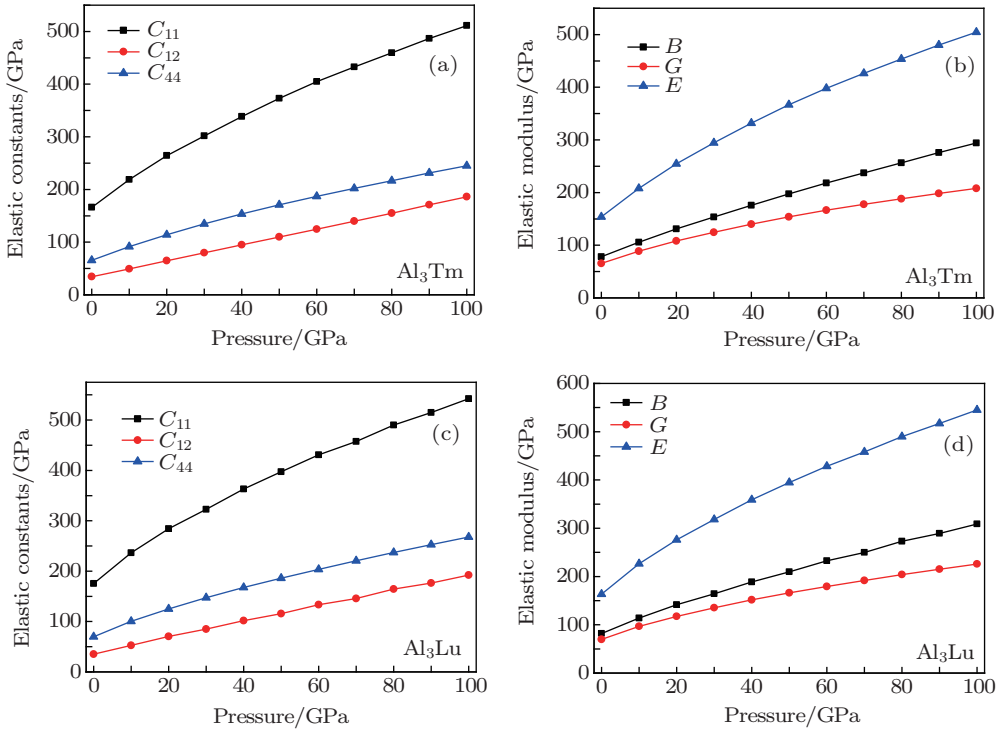



**Fig. 4.** (color online) Elastic constants and elastic moduli of $Al_3Tm$ and $Al_3Lu$ at different pressures.

The elastic anisotropy constant is an important parameter of material and has many industrial and technological applications. Based on calculated elastic constants and moduli, we employ three methods to estimate the anisotropies for $L1_2$ $Al_3Tm$, and $Al_3Lu$. Zener factor $A^Z$, Chung–Buessem anisotropy index $A^G$, and universal elastic anisotropy index $A^U$ have been proposed as follows:[30–32]

$$A^Z = \frac{2C_{44}}{C_{11} - C_{12}}, \tag{4}$$

$$A^{\mathrm{G}} = \frac{G_{\mathrm{V}} - G_{\mathrm{R}}}{G_{\mathrm{V}} + G_{\mathrm{R}}}, \tag{5}$$

$$A^{\mathrm{U}} = 5\frac{G_{\mathrm{V}}}{G_{\mathrm{R}}} + \frac{B_{\mathrm{V}}}{B_{\mathrm{R}}} - 6 \geq 0. \tag{6}$$

The calculated dependences of anisotropic factors ($A^{\mathrm{Z}}$, $A^{\mathrm{G}}$, $A^{\mathrm{U}}$) on pressure for $Al_3Tm$ and $Al_3Lu$ are shown in Fig. 5. It is noted that the various tendencies of $A^{\mathrm{Z}}$, $A^{\mathrm{G}}$, and $A^{\mathrm{U}}$ are very similar for two compounds. For the Chung–Buessem anisotropy index $A^{\mathrm{G}}$, 1 represents the largest anisotropy and 0 refers to elastic isotropy. The $A^{\mathrm{G}}$ values of $Al_3Tm$ and $Al_3Lu$ deviate from 0 with increasing pressure, indicating that they are anisotropic. The universal elastic anisotropy index $A^{\mathrm{U}}$ is equal to zero, namely the crystal with the value of $A^{\mathrm{U}} = 0$ is elastically isotropic. At 0 GPa, the values of $A^{\mathrm{U}}$ for $Al_3Tm$ and $Al_3Lu$ are close to 0, indicating that they are both isotropic. However, the values of $Al_3Tm$ and $Al_3Lu$ deviate from 0 as pressure increases, indicating that they are anisotropic. For the Zener factor $A^{\mathrm{Z}}$, the vales of $Al_3Tm$ and $Al_3Lu$ deviate from 1 with the increase of pressure, and we can also regard $Al_3Tm$ and $Al_3Lu$ as being elastically anisotropic under high pressure. In Fig. 5, the values of $A^{\mathrm{Z}}$, $A^{\mathrm{G}}$, and $A^{\mathrm{U}}$ of $Al_3Lu$ are larger than those of $Al_3Tm$. It indicates that both $Al_3Tm$ and $Al_3Lu$ exhibit anisotropy. In the meantime, the anisotropy increases with the increasing of pressure, and $Al_3Lu$ has more of an anisotropic feature than $Al_3Tm$ in the whole pressure range.

In order to further describe the elastic anisotropies for $Al_3Tm$ and $Al_3Lu$, we plot the three-dimensional (3D) curved surface of Young's modulus $E$ in a given direction. The surface of 3D Young's modulus $E$ can be determined by using the following equation:[33]

$$\frac{1}{E} = S_{11} - 2\left(S_{11} - S_{12} - \frac{S_{44}}{2}\right)\left(l_1^2 l_2^2 + l_2^2 l_3^2 + l_1^2 l_3^2\right). \tag{7}$$

In Eq. (7), the constants $S_{11}$, $S_{12}$, and $S_{44}$ are the elastic compliance constants. $l_1$, $l_2$, and $l_3$ are the direction cosines

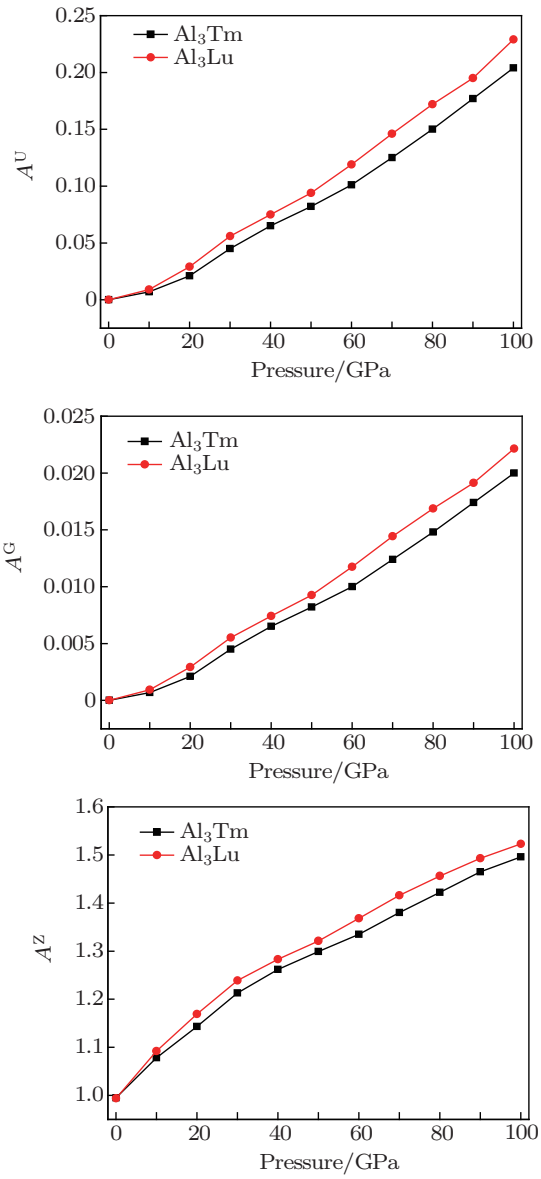



**Fig. 5.** (color online) Pressure dependences of anisotropic factors ($A^{\mathrm{U}}$, $A^{\mathrm{G}}$, $A^{\mathrm{Z}}$) for $Al_3Tm$ and $Al_3Lu$.

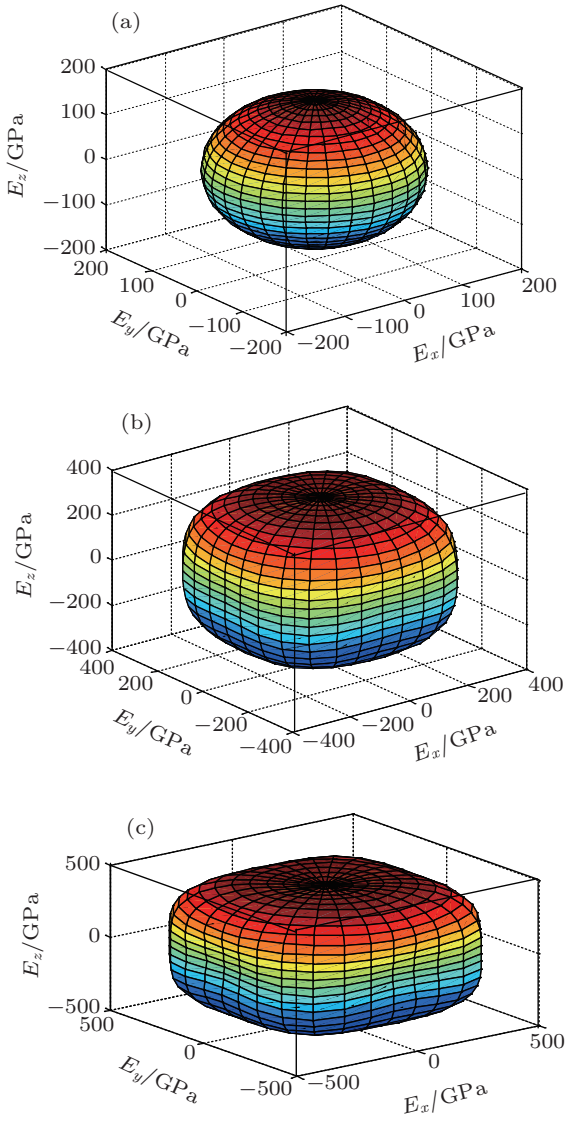



**Fig. 6.** (color online) Directional dependences of Young's modulus for $Al_3Tm$ at 0 GPa (a), 50 GPa (b), and 100 GPa (c), the axes are in units of GPa.

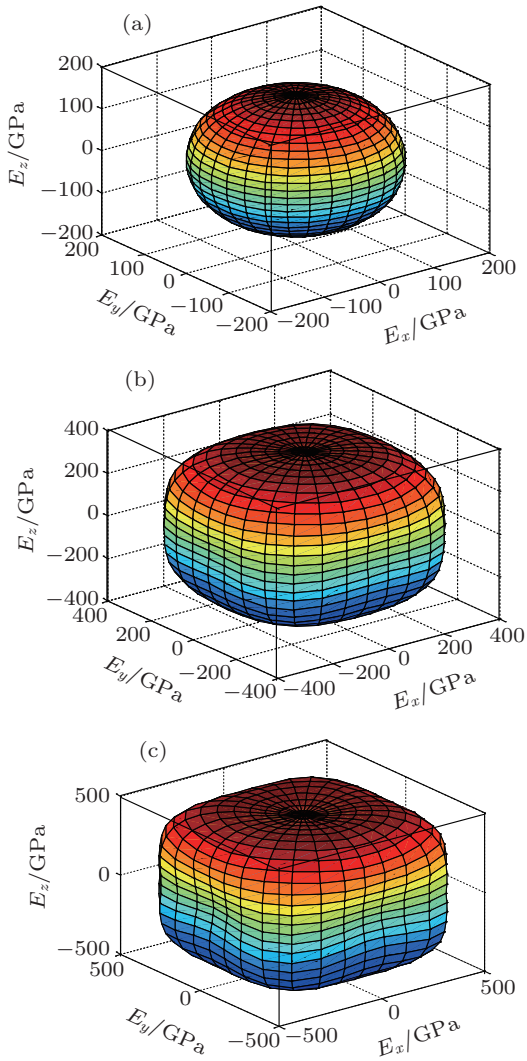



**Fig. 7.** (color online) Directional dependences of Young's modulus for $Al_3Lu$ at 0 GPa (a), 50 GPa (b), and 100 GPa (c), the axes are in units of GPa.

between the loading direction and three coordinate axes. $S_{ij}$s are obtained from the inverse of the matrix of the elastic constants $C_{ij}$. For an isotropic material, the 3D curved surface should exhibit a spherical shape. In the meantime, the deviation degree from the spherical surface indicates the extent of anisotropy. The 3D figures of $Al_3Tm$ and $Al_3Lu$ under different pressures are plotted in Figs. 6 and 7. In Figs. 6 and 7, each of the 3D surfaces of the $Al_3Tm$ and $Al_3Lu$ at 0 GPa obviously has a spherical shape and exhibits a noticeable isotropy. The degrees of deviation from the sphere for $Al_3Tm$ and $Al_3Lu$ increase with increasing pressure, which indicates that each Young's moduli for $Al_3Tm$ and $Al_3Lu$ shows an increasing elastic anisotropy under high pressure. In the meantime, we can note that the degree of deviation from the spherical surface of $Al_3Lu$ is slightly bigger than that of $Al_3Tm$ under high pressure, which indicates that $Al_3Lu$ has slightly bigger anisotropy than $Al_3Tm$. We can note that this result is consistent with the analyses of anisotropy factors ($A^Z, A^G, A^U$) under high pressure. As pressure increases, we can see that the elastic anisotropy becomes bigger under high pressure. The phenomenon results from the shorter bond length with increasing pressure. The shorter bond can lead to the larger force constants, which will make $Al_3Tm$ and $Al_3Lu$ more anisotropic.

### 3.3. Anisotropic sound velocity and Debye temperature under pressure

The sound velocities in solids are related to their elastic constants, thermal conductivities, and phonon frequencies. For $L1_2$, $Al_3Tm$, and $Al_3Lu$, we calculate the sound velocities of longitudinal ($v_l$) and transverse waves ($v_t$) along the [100], [110], and [111] crystal directions. We calculate sound velocities by using the following equations:[34,35]

$$v_l = [(B+4G/3)/\rho]^{1/2}, \quad v_t = (G/\rho)^{1/2}, \tag{8}$$

$$[100]v_l = \sqrt{C_{11}/\rho}, \quad [100]v_{t1} = [100]v_{t2} = \sqrt{C_{44}/\rho}, \tag{9}$$

$$[110]v_l = \sqrt{\left[C_{44} + \frac{1}{2}(C_{11}+C_{12})\right]/\rho}, \tag{10}$$

$$[1\bar{1}0]v_{t1} = \sqrt{(C_{11}-C_{12})/2\rho}, \quad [110]v_{t2} = \sqrt{C_{44}/\rho}, \tag{11}$$

$$[11\bar{2}]v_{t1} = [11\bar{2}]v_{t2} = \sqrt{(C_{11}-C_{12}+C_{44})/3\rho}, \tag{12}$$

$$[111]v_t = \sqrt{(C_{11}+2C_{12}+4C_{44})/3\rho}. \tag{13}$$

**Table 3.** Sound velocities along different directions (km/s) and for different values of $\rho$(g/cm$^3$) for $L1_2$, $Al_3Tm$, and $Al_3Lu$ at different pressures (GPa).

| | | | [100] | | [110] | | | [111] | |
|---|---|---|---|---|---|---|---|---|---|
| Al | $P$ | $\rho$ | $[100]v_l$ | $[001]v_{t1,2}$ | $[110]v_l$ | $[110]v_t$ | $[001]v_t$ | $[111]v_l$ | $[112]v_{t1,2}$ |
| Present | 0 | 2.732 | 6.006 | 3.358 | 6.239 | 4.193 | 3.325 | 6.318 | 3.052 |
| Exp.[37] | 0 | – | 6.325 | 3.220 | 6.469 | 4.128 | 3.220 | 6.157 | 3.023 |
| $Al_3Tm$ | $P$ | $\rho$ | $[100]v_l$ | $[001]v_{t1,2}$ | $[110]v_l$ | $[110]v_t$ | $[001]v_t$ | $[111]v_l$ | $[112]v_{t1,2}$ |
| | 0 | 5.521 | 5.401 | 3.418 | 5.429 | 3.373 | 3.418 | 5.438 | 3.388 |
| | 10 | 6.114 | 5.980 | 3.868 | 6.070 | 3.725 | 3.868 | 6.100 | 3.773 |
| | 20 | 6.572 | 6.340 | 4.167 | 6.509 | 3.897 | 4.167 | 6.564 | 3.989 |
| | 30 | 6.963 | 6.583 | 4.398 | 6.836 | 3.993 | 4.398 | 6.919 | 4.132 |
| | 40 | 7.311 | 6.802 | 4.584 | 7.116 | 4.080 | 4.584 | 7.217 | 4.255 |
| | 50 | 7.628 | 6.993 | 4.734 | 7.352 | 4.154 | 4.734 | 7.468 | 4.356 |
| | 60 | 7.913 | 7.151 | 4.859 | 7.554 | 4.206 | 4.859 | 7.683 | 4.434 |
| | 70 | 8.179 | 7.273 | 4.970 | 7.726 | 4.232 | 4.970 | 7.871 | 4.491 |
| | 80 | 8.429 | 7.384 | 5.069 | 7.884 | 4.251 | 5.069 | 8.043 | 4.540 |
| | 90 | 8.675 | 7.489 | 5.164 | 8.034 | 4.266 | 5.164 | 8.208 | 4.585 |
| | 100 | 8.894 | 7.581 | 5.248 | 8.168 | 4.276 | 5.248 | 8.354 | 4.623 |

**Table 3.** (*Continued*).

| | | | [100] | | [110] | | | [111] | |
|---|---|---|---|---|---|---|---|---|---|
| Al | $P$ | $\rho$ | [100]$v_{\rm l}$ | [001]$v_{\rm t1,2}$ | [110]$v_{\rm l}$ | [110]$v_{\rm t}$ | [001]$v_{\rm t}$ | [111]$v_{\rm l}$ | [112]$v_{\rm t1,2}$ |
| $Al_3Lu$ | $P$ | $\rho$ | [100]$v_{\rm l}$ | [001]$v_{\rm t1,2}$ | [110]$v_{\rm l}$ | [110]$v_{\rm t}$ | [001]$v_{\rm t}$ | [111]$v_{\rm l}$ | [112]$v_{\rm t1,2}$ |
| | 0 | 5.686 | 5.347 | 3.401 | 5.389 | 3.334 | 3.401 | 5.403 | 3.356 |
| | 10 | 6.049 | 6.079 | 3.960 | 6.186 | 3.897 | 3.960 | 6.222 | 3.847 |
| | 20 | 6.595 | 6.427 | 4.263 | 6.628 | 4.027 | 4.263 | 6.694 | 4.052 |
| | 30 | 7.05 | 6.655 | 4.480 | 6.942 | 4.107 | 4.480 | 7.035 | 4.198 |
| | 40 | 7.437 | 6.889 | 4.681 | 7.231 | 4.191 | 4.681 | 7.341 | 4.323 |
| | 50 | 7.797 | 7.061 | 4.830 | 7.451 | 4.249 | 4.830 | 7.577 | 4.422 |
| | 60 | 8.140 | 7.220 | 4.961 | 7.664 | 4.275 | 4.961 | 7.807 | 4.494 |
| | 70 | 8.429 | 7.315 | 5.079 | 7.816 | 4.299 | 5.079 | 7.976 | 4.555 |
| | 80 | 8.716 | 7.457 | 5.186 | 8.002 | 4.321 | 5.186 | 8.176 | 4.613 |
| | 90 | 8.98 | 7.540 | 5.280 | 8.127 | 4.340 | 5.280 | 8.314 | 4.664 |
| | 100 | 9.246 | 7.641 | 5.368 | 8.267 | 4.353 | 5.368 | 8.466 | 4.709 |

The calculated sound velocities along three directions of Al, $Al_3Tm$, and $Al_3Lu$ are presented in Table 3. These calculated values of Al in this work are in good agreement with the available calculated and experimental results.[36,37] We can note that compounds with smaller densities and larger elastic constants exhibit larger sound velocities. The sound velocities along different directions at different pressures for $Al_3Tm$ and $Al_3Lu$ are shown in Fig. 8. We can note that the sound velocities in the directions increase with the increasing of pressure in Fig. 8. At a given pressure, the corresponding sound velocities in different directions of $Al_3Tm$ are smaller than those of $Al_3Lu$.

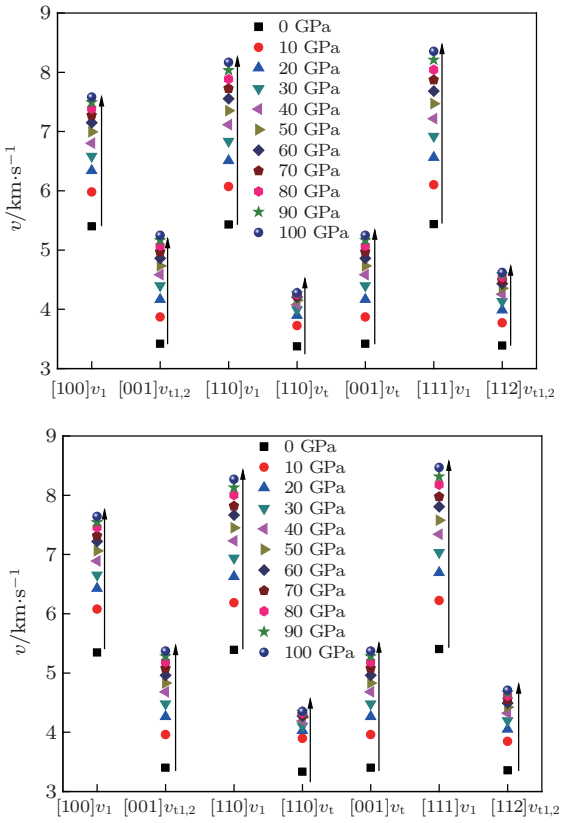



**Fig. 8.** (color online) Sound velocities along different directions for $Al_3Tm$ (a) and $Al_3Lu$ (b), each as a function of pressure.

The Debye temperature is an important parameter describing the material thermodynamic properties in solid state physics. We calculate the Debye temperatures of $Al_3Tm$ and $Al_3Lu$ by using the average sound velocities from the following equations:[37]

$$\Theta_{\rm D} = \frac{h}{k_{\rm B}}\left[\frac{3n}{4\pi}\left(\frac{N_A\rho}{M}\right)\right]^{1/3} v_{\rm m}, \tag{14}$$

$$v_{\rm m} = \left[\frac{1}{3}\left(\frac{2}{v_t^3}+\frac{1}{v_{\rm l}^3}\right)\right]^{-1/3}, \tag{15}$$

where $h$ is the Planck constant, $N_{\rm A}$ is the Avogadro number, $M$ is the molecular weight, $\rho$ is the density, $k_{\rm B}$ is the Boltzmann constant, $n$ is the number of atoms per formula unit, and $v_{\rm m}$ is the average sound velocity. The calculated values of sound velocity and Debye temperature $\Theta_{\rm D}$ of Al, $Al_3Tm$, and $Al_3Lu$ are listed in Table 4. In Table 4, the calculated values of the present work are also in good agreement with the available calculated and experimental results.[12,36–38] From Table 4, we can note that the elastic wave velocities of $Al_3Tm$ and $Al_3Lu$ increase with increasing pressure. At high pressure, the increases of sound velocities become slower. We can also note that Debye temperatures of $Al_3Tm$ and $Al_3Lu$ increase with increasing pressure in Table 4. To describe the dependences of Debye temperature on the applied pressure, a nonlinear three-order polynomial is fitted up to 100 GPa. The polynomials obtained for $L1_2$ structures $Al_3Tm$ and $Al_3Lu$ are respectively as follows:

$$\Theta_{\rm DAl_3Tm} = 410.89 + 7.58P - 6.25\times10^{-2}P^2 + 2.56\times10^{-4}P^3,$$
$$\Theta_{\rm DAl_3Lu} = 404.56 + 7.32P - 5.87\times10^{-2}P^2 + 2.41\times10^{-4}P^3.$$

We can note that the values of zero-pressure Debye temperature $\Theta_{\rm D}$ are 411 K and 404 K for $Al_3Tm$ and $Al_3Lu$ respectively. The errors between the fitting $\Theta_{\rm D}$ and calculated $\Theta_{\rm D}$ in Table 3 are less than 1%. It indicates that the relationships between $\Theta_{\rm D}$ and pressure for $Al_3Tm$ and $Al_3Lu$ are reliable. In the meantime, $Al_3Tm$ possesses a higher Debye

temperature than $Al_3Lu$ in the whole pressure range. The increases of $\Theta_D$ correspond to normal vibrations of $Al_3Tm$ and $Al_3Lu$ strengthening with pressure rising.

**Table 4.** Elastic wave velocities (m/s) and the Debye temperatures (K) for Al, $Al_3Tm$, and $Al_3Lu$.

| | | $v_l$ | $v_t$ | $v_m$ | $\Theta_D$ |
|---|---|---|---|---|---|
| Al | Present | 6129 | 3348 | 3739 | 423 |
| | Cal.[a] | 6127 | 3339 | 3725 | 433 |
| | Exp.[b,c] | 6229 | 3338 | 3796 | 428 |
| $Al_3Tm$ | Cal.[d] | 5396 | 3442 | 3684 | 412 |
| Present | 0 | 5480 | 3448 | 3810 | 411 |
| | 10 | 6051 | 4194 | 4057 | 487.8 |
| | 20 | 6472 | 4468 | 4231 | 544.86 |
| | 30 | 6779 | 4662 | 4375 | 591.33 |
| | 40 | 7042 | 4822 | 4493 | 631.22 |
| | 50 | 7267 | 4955 | 4586 | 666.40 |
| | 60 | 7456 | 5060 | 4660 | 697.96 |
| | 70 | 7614 | 5146 | 4724 | 726.76 |
| | 80 | 7758 | 5218 | 4783 | 753.93 |
| | 90 | 7895 | 5286 | 4834 | 777.93 |
| | 100 | 8015 | 5345 | 3810 | 800.99 |
| $Al_3Lu$ | Cal.[d] | 5291 | 3258 | 3595 | 404 |
| Present | 0 | 5306 | 3278 | 3627 | 401 |
| | 10 | 4082 | 3691 | 4082 | 476.38 |
| | 20 | 4349 | 3932 | 4349 | 531.86 |
| | 30 | 4545 | 4108 | 4545 | 577.23 |
| | 40 | 4708 | 4253 | 4708 | 616.76 |
| | 50 | 4836 | 4369 | 4836 | 652.07 |
| | 60 | 4939 | 4459 | 4939 | 683.73 |
| | 70 | 5028 | 4538 | 5028 | 712.98 |
| | 80 | 5110 | 4610 | 5110 | 741.14 |
| | 90 | 5180 | 4673 | 5180 | 765.39 |
| | 100 | 5246 | 4731 | 5246 | 789.24 |

[a]Ref. [36], [b]Ref. [37], [c]Ref. [38], [d]Ref. [12].

### 3.4. Thermodynamic properties

We calculate the thermodynamic properties of $Al_3Tm$ and $Al_3Lu$ by using the quasi-harmonic approximation (QHA) theory. In order to verify the correctness of the computational method, we calculate the values of Gibbs free energy ($G$) and enthalpy ($H$) of pure Tm, Lu, $Al_3Tm$, and $Al_3Lu$ at 0 GPa. In Figs. 9 and 10, we can note that our calculated results for Tm and Lu agree well with the available experimental values reported by Barin.[39] It indicates that our method is reasonable. In Fig. 9, we can note that the Gibbs free energy curves are similar to each other and move down with increasing temperature for $Al_3Tm$ and $Al_3Lu$. The smaller the values of Gibbs free energy, the better the thermal stability of material will be. So $Al_3Tm$ has the better thermal stability than $Al_3Lu$ in a temperature range from 0 K to 1000 K. Figure 10 shows the linear variations of enthalpy ($H$) with temperature for $Al_3Tm$ and $Al_3Lu$ at 0 GPa. In order to further discuss the thermodynamic properties, we also calculate the thermal expansion coefficient $\alpha$, specific heat capacity $C_P$, and entropy $S$. The thermal expansion coefficients $\alpha$ under high pressure are shown in Fig. 11. In the low temperature region ($T < 300$ K), the coefficient increases rapidly with increasing temperature and then increases smoothly and slowly at high temperatures. The thermal expansion becomes slower with the increase of pressure and keeps unchanged basically at high temperature. Figure 11 also shows the calculated values of specific heat capacity $C_P$ of $Al_3Tm$ and $Al_3Lu$. At 0 GPa, the values of $C_P$ are proportional to $T^3$ in the low temperature range and become linear with the increase of temperature in the high temperature range. At high pressure, $C_P$ keeps unchanged with increasing temperature.

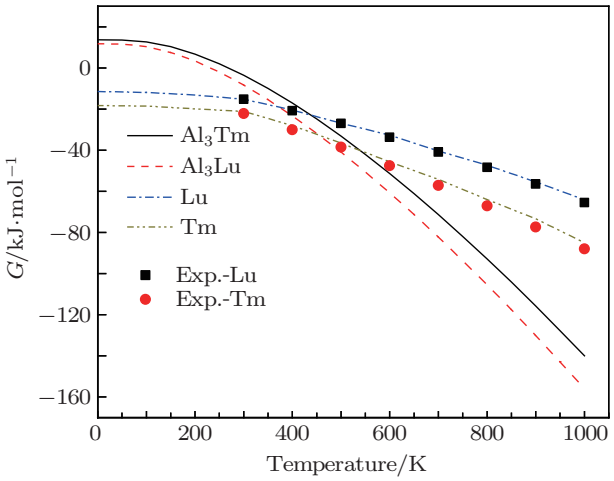



**Fig. 9.** (color online) Temperature dependences of Gibbs free energy for Tm, Lu, $Al_3Tm$, and $Al_3Lu$ at 0 GPa.

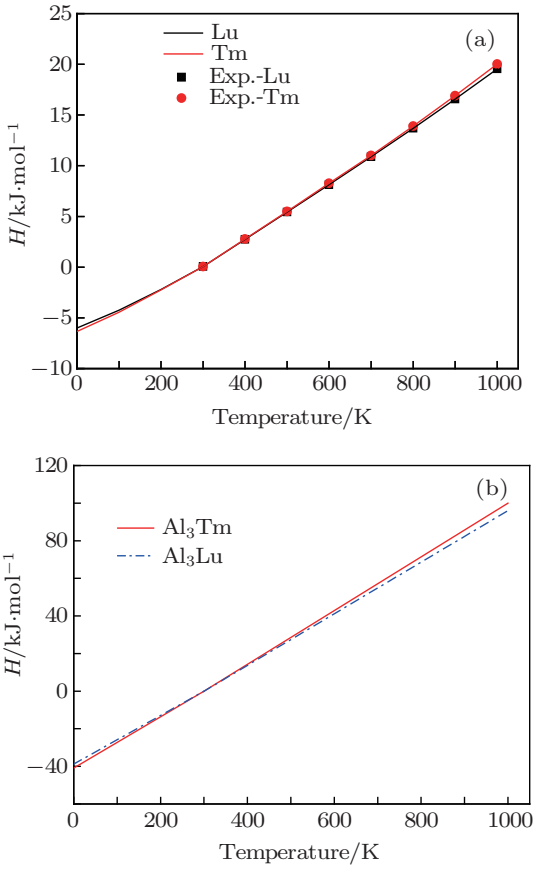



**Fig. 10.** (color online) Temperature dependences of enthalpy for Tm, Lu (a), $Al_3Tm$ and $Al_3Lu$ (b).

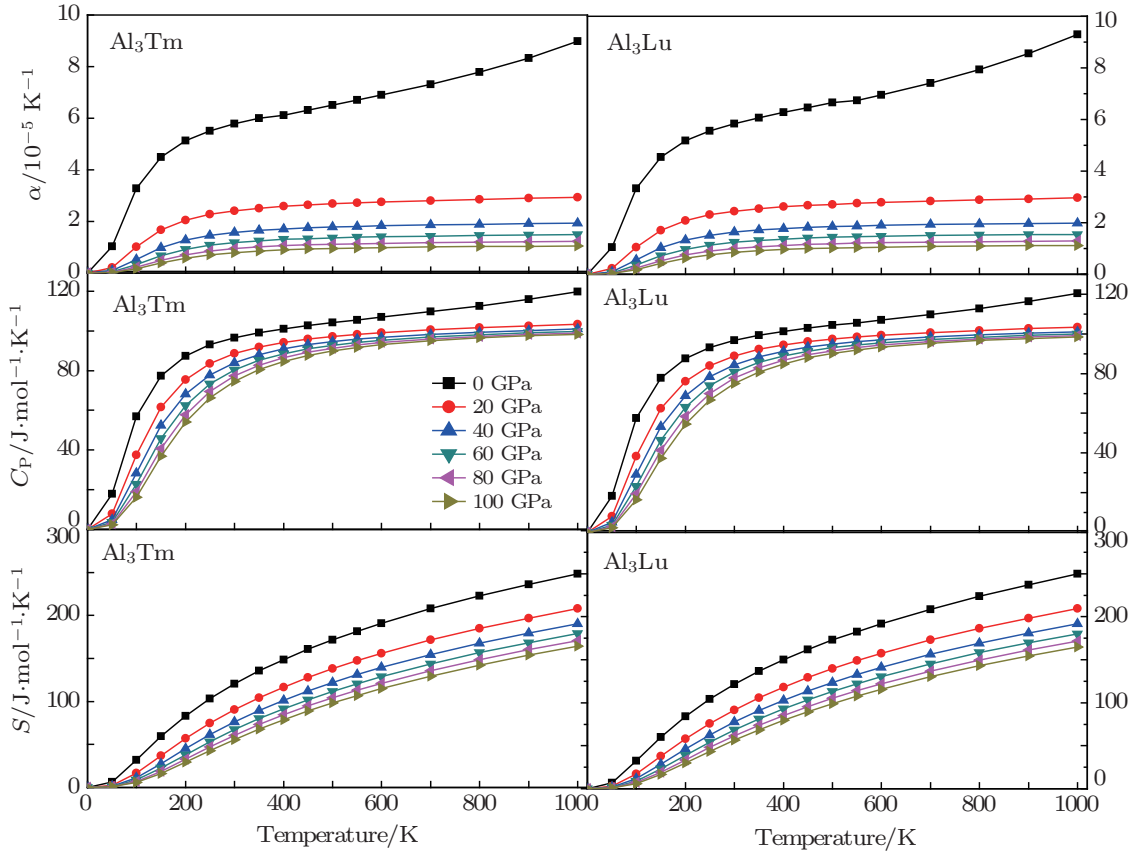



**Fig. 11.** (color online) Temperature dependences of thermal parameters for $Al_3Tm$ and $Al_3Lu$.

It indicates that the increasing of pressure influences the increase of $C_P$. The curves of entropy $S$ at different pressures are shown in Fig. 11. The curves indicate that the entropy decreases with the increase of pressure at a given temperature. Unlike the constant pressure heat capacity $C_P$, the high temperature dependence of entropy $S$ is nearly insensitive to pressure. These results indicate that the effects of increasing pressure and reducing temperature on $Al_3Tm$ and $Al_3Lu$ are the same.

## 4. Conclusions

In this work, the dynamic stabilities, elastic and thermodynamic properties of $Al_3Tm$ and $Al_3Lu$ under high pressure are investigated by using first-principles calculations. According to the vibrational properties, we can predict that $Al_3Tm$ and $Al_3Lu$ will keep the lattice stable up to 100 GPa. The elastic constants and elastic moduli for $Al_3Tm$ and $Al_3Lu$ indicate that the two compounds keep mechanically stable and possess a brittle nature in the considered pressure range. The calculated anisotropic constants $A^G$, $A^U$, and $A^Z$ and 3D curved surface of Young's modulus show that $Al_3Tm$ and $Al_3Lu$ are both isotropic at 0 GPa and are anisotropic under high pressure. The sound velocities in different directions and Debye temperatures under high pressure are also calculated for both phases. We also calculate the thermodynamics properties by the QHA method and discuss the relationships between these thermal parameters and pressure as well.

## References


[1] Watanabe C, Kondo T and Monzen R 2004 *Metall. Mater. Trans. A* **35** 3003
[2] Knipling K E, Dunand D C and Seidman D N 2007 *Microscopy and Microanalysis* **13** 503
[3] Wen S P, Gao K Y, Li Y, Huang H and Nie Z R 2011 *Scripta Mater.* **65** 592
[4] Booth-Morrison C, Dunand D C and Seidman D N 2011 *Acta Mater.* **59** 7029
[5] Karnesky R A, Dunand D C and Seidman D N 2009 *Acta Mater.* **57** 4022
[6] van Dalen M E, Gyger T, Dunand D C, and Seidman D N 2011 *Acta Mater.* **59** 7615
[7] Karnesky R A, van Dalen M E, Dunand D C and Seidman D N 2006 *Scripta Mater.* **55** 437
[8] van Dalen M E, Karnesky R A, Cabotaje J R, Dunand D C and Seidman D N 2009 *Acta Mater.* **57** 4081
[9] Knipling K E, Dunand D C and Seidman D N 2006 *Zeitschrift fur Metallkunde* **97** 246
[10] Tsvyashchenko A V, Fomicheva L N, Brudanin V B, Kochetov O I, Salamatin A V, Velichkov A and Wiertel M 2007 *Solid State Commun.* **142** 664
[11] Krug M E, Werber A, Dunand D C and Seidman D N 2010 *Acta Mater.* **58** 134
[12] Tao X M, Ouyang Y, Liu H and Feng Y 2008 *Int. J. Mater. Res.* **99** 582
[13] Shi S Q, Tanaka S and Kohyama M 2007 *Phys. Rev. B* **76** 075431
[14] Zhang H, Tang Y, Shen J, Xin X and Cui L 2011 *Appl. Phys. A* **104** 529
[15] Shang S L, Hector L G Jr, Shi S Q, Qi Y, Wang Y and Liu Z K 2012 *Acta Mater.* **60** 5204
[16] Ouyang C, Du Y, Shi S Q and Lei M S 2009 *Phys. Lett. A* **373** 2796
[17] Tang Y H, Zhang H, Cui L X, Ouyang C, Shi S Q, Tang W H, Li H, Lee J and Chen L 2010 *Phys. Rev. B* **82** 125104
[18] Shi S Q, Qi Y, Li H and Hector L G Jr 2013 *J. Phys. Chem. C* **117** 8579

[19] Shi S Q, Lu P, Liu Z, Qi Y, Hector L G Jr, Li H and Harris S J 2012 *J. Am. Chem. Soc.* **134** 15476
[20] Li Z L and Cheng X L 2014 *Chin. Phys. B* **23** 046201
[21] Lu C, Jin X L and Su T C 2014 *Chin. Phys. B* **23** 026201
[22] Kresse G and Furthmuller J 1996 *Comput. Mater. Sci.* **6** 15
[23] Togo A, Phonopy, http://phonopy.sourceforge.net/
[24] Vinet P, Rose J, Ferrante J and Smith J 1989 *J. Phys.: Condens. Matter* **1** 1941
[25] Dederichs P H, Schober H and Sellmyer D J 1981 *Phonon states of elements. Electron states and Fermi surfaces of alloys* (Berlin/Heidelberg: Springer)
[26] Liu Z L, Yang J H, Cai L C, Jing F Q and Alfe D 2011 *Phys. Rev. B* **83** 144113
[27] Shang S, Wang Y and Liu Z K 2007 *Appl. Phys. Lett.* **90** 101909
[28] Hill R W 1952 *Proc. Phys. Soc. London* **65A** 349
[29] Pugh S F 1954 *Philos. Mag.* **45** 823
[30] Spoor P, Maynard J and Kortan A 1995 *Phys. Rev. Lett.* **75** 3462
[31] Ranganathan S I and Ostoja-Starzewski M 2008 *Phys. Rev. Lett.* **101** 055504
[32] Chung D and Buessem W 1967 *J. Appl. Phys.* **38** 2010
[33] Peng M J, Duan Y H and Sun Y 2015 *Comput. Mater. Sci.* **98** 311
[34] Belmonte D, Ottonello G and Vetuschi Zuccolini M 2014 *American Mineralogist* **99** 1449
[35] Ottonello G, Civalleri B, Ganguly J, Perger W F, Belmonte D and Vetuschi Zuccolini M 2010 *American Mineralogist* **95** 563
[36] Feng J, Xiao B, Wan C L, Qu Z X, Huang Z C, Chen J C, Zhou R and Pan W 2011 *Acta Mater.* **59** 1742
[37] Grimvall G 1999 *Thermo Physical Properties of Materials* (Amsterdam: North Holland)
[38] Feng J, Xiao B, Zhou R, Pan W and Clarke D R 2012 *Acta Mater.* **60** 3380
[39] Barin I 1995 *Thermochemical Date of Pure Substance* (New York: VCH) pp. 990, 1717